INVESTIGATION OF ADHESIVELY BONDED COMPOSITE STRUCTURE JOINTS

Nadia Basso[1], Maajid Chishti[2], Javid Bayandor[2], Rodney Thomson[3], Chiara Bisagni[1]

[1]Politecnico di Milano
Dipartimento di Ingegneria Aerospaziale
Via la Masa 34, 20156 Milano, Italy
[2]The Sir Lawrence Wackett Aerospace Centre
[2]School of Aerospace, Mechanical and Manufacturing Engineering
Royal Melbourne Institute of Technology, Melbourne, VIC, Australia
[3]Cooperative Research Centre for Advanced Composite Structures Limited, Melbourne, VIC, Australia
*E-mail: **Javid.Bayandor@rmit.edu.au***

Keywords: *Composite bonded joints, FEM, mode I, mode II, single lap joints*

Abstract

A series of tests and simulations were constructed around representative bonded joint samples. The specimens were manufactured and tested under fracture modes I and II. The orientation of the mid-planar interfaces plies between the adherends and the adhesive were altered to determine the role of interfacial bonding on fracture mechanism. For mode I test, it was found that different orientation did not influence the energy delivered to create a unit area of fresh fracture surface. mode II tests were conducted on release film and natural crack specimens. The results of the analysis showed that the specimens with release film produced more conservative and lower values of G_{IIC} with respect to natural crack specimen. The curves obtained from the finite element modelling simulation of single lap joint gave good agreement with experimental tests.

1 Introduction

The use of mechanical fasteners in connecting two similar or dissimilar materials is well known in the literature. Metal alloys have been used as major manufacturing constituents for aircraft, with components mostly riveted or fastened together to avoid possible local joint imperfections and crack initiations, often associated with welded (spot, seam) joints.

Due to the ever increasing demand for lighter and more efficient aircraft, composites have begun to be extensively used in primary aerospace structural components in addition to secondary structures. This is the impetus behind the extensive research being conducted in the field of composite joint responses under loading. Adhesively bonded composite joints are considered more efficient than fastened composite joints, because of their minimal sources of stress concentrations, smooth load transfer, superior fatigue resistance and improved damage tolerance [1]. Factors such as poor surface preparation, moisture ingression, aging, unpredictable crack propagation patterns etc. can lead to poor joint performance. Statistics show that approximately 70% of the failure of structures is initiated from joints [3]. To reduce the possibility of failure, it is important to understand the failure mechanism of composite joints. Hiley [4] studied the relationship between modes I and II energy release rates and ply orientation in controlling the delamination growth in co-cured specimens. Yan et al. [5] investigated the role of bond line thickness in the fracture behaviour of adhesive joints in composite, concluding that the crack tip stress field is affected by bond thickness. Hart-Smith [6] provided significant contribution

to understand the behaviour of single lap bonded joints, extending the classical elastic-solution first published by Volkersen [7].

Experimental tests and explicit Finite Element (FE) simulations were carried out to analyse the stress fields inside the single lap joints. The current work analyses the process that brings fast and simple predictive methodologies to implementation, from experimental trial to numerical modelling. It is intended to consider single lap shear tests as a combination of modes I and II stress field and develop a FE model which uses the values of energy release rates from the modes I and II. A sensitivity study of different ply orientations in co-cured specimens was also performed and reported.

2 Experimental Trials

All the specimens were prepared using plain weave carbon fiber epoxy prepregs. The laminates were bonded using an adhesive film FM 1515-3. Tables 1 and 2 provide the mechanical properties of the prepreg and adhesive film, respectively.

Table 1 Prepreg properties

Cycom 970/PWC ST (CCF) 60" resin tack level 9	
Young's modulus (E_{11}=E_{12})	55 *GPa*
Shear modulus (G_{12})	5.0 *GPa*
0° Tensile strength	740 *MPa*

Table 2 Adhesive properties

FM 1515-13 Adhesive film	
Young's Modulus	1.00 *GPa*
Shear Modulus	0.38 *GPa*
Poisson's Ratio	0.3

Figure 1 shows the setup of the vacuum bagging process used to manufacture the composite laminate.

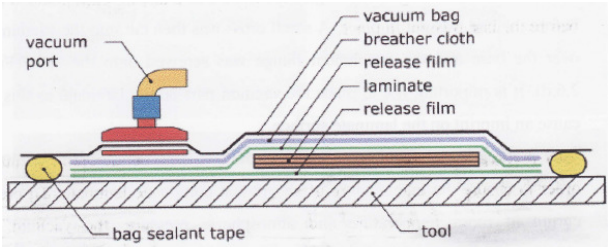

Fig. 1. Vacuum bagging

Extra care was taken to ensure that aluminium plate tool was free from any irregularity which could damage the laminate. The laminates were cured in an autoclave.

Figure 2 shows the temperature and pressure curing cycle used for manufacturing the composite laminates. These laminates were used to manufacture the joints tested during this study. The autoclave curing process of the joint is shown in Fig. 3. A release film of the same thickness as the adhesive was used to generate the initial crack, i.e. to ensure that the crack starts to propagate from an exact point at the interface, as suggested by the standards.

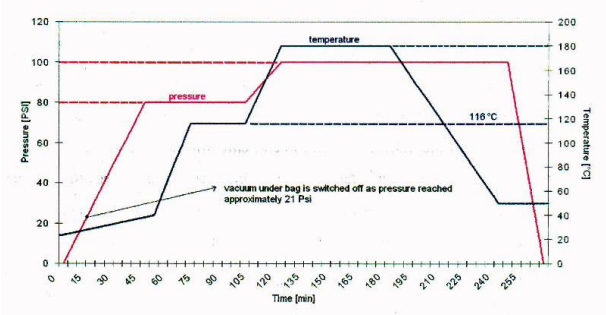

Fig. 2. Laminate curing time line

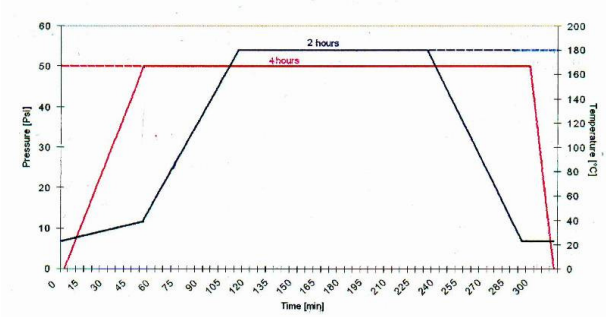

Fig. 3. Joint curing time line

2.1 Specimen Specification

Modes I and II specimens were prepared based on the standards in [8] and [9], respectively. To realise different interface orientations between adherend and adhesive, two different stacking sequences, A and B, were used. Three different ply orientations at the mid plane were selected; $0^o/0^o$, $0^o/45^o$ and $45^o/45^o$.

In order to distinguish between single lap, mode I and mode II specimens and between the different cases studied, a specimen labelling code was established. This system indicates which of the three tests methods were used,

containing a number to identify each specimen. The code for Double Cantilever Beam (DCB) and End Notch Flexural (ENF) specimens is explained in Table 3. Similarly, Table 4 explains the code for single lap specimens.

Table 3 Specimen code for modes I and II

Position in the code	Definition	Code	Description
1	Loading method	**I**	Mode I
		II	Mode II
2	Interface orientation	**A**	$0^o/0^o$
		B	$45^o/45^o$
		C	$0^o/45^o$
3	Specimen number	**1-4**	Specimens per test

Table 4 Specimen code for single lap joint

Position in the code	Definition	Code	Description
1	Overlap length	**A**	12.5 *mm*
		B	25 *mm*
		C	37.5 *mm*
2	Specimen number	**1-3**	Specimens per test

For example 'IC3' explains that a mode I test was conducted with 0/45 degree interface orientation on the third specimen. Metallic hinges with thickness of 1 *mm* were bonded with high peel strength glue (Araldite 420A and hardener 420B), as recommended by Ref. [8].

Three thickness measurements distributed over the specimens were made using a flat-face micrometer and the average was recorded. Table 5 shows the dimensions used for mode I specimens during the manufacturing process.

Table 5 Dimensions of DCB specimens

	L (*mm*)	w (*mm*)	h (*mm*)	l_1 (*mm*)
IA1-4	250	25.00	3.03	25.00
IB1	250	25.00	3.03	**23.35**
IB2	250	25.15	3.02	**27.69**
IB3	250	25.00	3.03	**27.83**
IB4	250	25.00	3.04	**29.07**
IC1-4	250	25.05	3.05	25.00

In order to obtain a more comprehensive understanding of the crack propagation mechanism, mode II tests were conducted on two types of specimens. The first type specimens were obtained from the previously failed mode I samples, with their test induced cracks. The specimens were cut from the residual part of the specimens tested in mode I according to [9]. These specimens were named as Natural Crack specimens. The second type specimens were manufactured to have an initial crack produced by the release film placed in the mid plane of the specimens. They were referred to as Release Film specimens. Table 6 provides the major dimensions of all mode II specimens.

Table 6 Dimensions of ENF specimens

	Code	t (*mm*)	w (*mm*)	l (*mm*)	c (*mm*)
Release Film	rIIA1-4	3.03	25.00	140	40
	rIIB1-4	3.03	25.00	140	40
	rIIC1-4	3.03	25.00	140	40
Natural Crack	nIIA1	3.03	25.00	156	40
	nIIA2	3.03	25.00	144	40
	nIIA3	3.03	25.00	136	40
	nIIA4	3.02	25.00	157.5	40
	nIIB1	3.04	25.00	152	40
	nIIB2	3.03	25.00	155	40
	nIIB3	3.03	25.05	161	40
	nIIB4	3.02	25.05	153	40
	nIIC1	3.07	25.05	159	40
	nIIC2	3.05	25.15	165	40
	nIIC3	3.04	25.15	163	40
	nIIC4	3.05	25.00	166.5	40

The single lap specimens used in the experiments were prepared according to the ASTM standards [10]. The same prepregs and adhesive, described earlier, were used to manufacture the single lap joints. The thickness of each substrate was 2.86 *mm*. In order to investigate the sensitivity of the joint to bonded area, specimens with 12.5 *mm*, 25 *mm* and 37.5 *mm* overlap lengths were manufactured and tested. The end tabs were introduced to reduce the eccentricity of the load path that causes out-of-plane bending moments, resulting in high

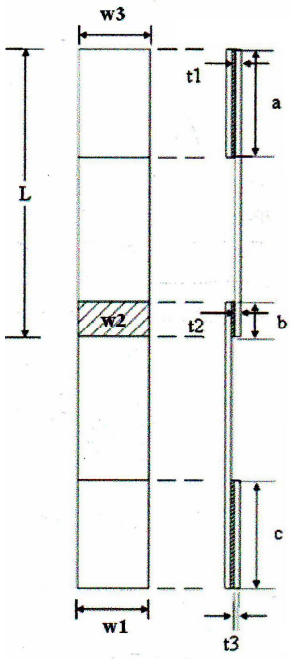

Fig. 4. Single lap joint

peel stresses and non-uniform shear stresses in the adhesive layer. Figure 4 shows a schematic of single lap joint. Tables 7 and 8 provide the dimensions of the single lap joints.

Table 7 Single lap specimen dimensions (*mm*)

	A	*b*	*c*	*w*1	*w*2	*w*3
A1-A3	37.6	12.5	37.3	24.75	24.94	25.24
B1-B3	38.7	25	36.72	25.18	24.88	24.5
C1-C3	36.5	37.5	37.70	25.55	25.55	25.33

Table 8 Single lap specimen dimensions (*mm*)

	*t*1	*t*2	*t*3	*L*
A1-A3	5.58	5.59	5.58	185
B1-B3	5.59	5.56	5.59	172
C1-C3	5.56	5.56	5.58	152.5

2.2 Experimental Procedure

To calculate the mode I fracture toughness energy, the German standards [8] were adopted. An Instron 5560 testing machine was used to test the specimen in all the loading cases. The machine is a 100 *kN* servo-hydraulic device to perform static or dynamic tests. One side of the specimens was coated with a thin layer of white resin to facilitate the crack length measurements. The mechanical properties of the adhesives are sensitive to the rate at which the load is applied. As the standards suggested, the specimens were loaded with a constant cross-head displacement rate of 10 *mm/min*. The load was continuously applied as peel-force until a crack length of 100 *mm* was achieved. The load versus crosshead displacement of the machine was recorded during the experiment. Interlaminar fracture toughness was calculated using [8]:

$$G_{IC} = \frac{A}{a * w} * 10^6 \qquad (1)$$

where: G_{IC} = Fracture toughness energy
A = Energy to obtain total propagated crack length [8]
a = Propagated crack length, less the initial crack length
w = Width of the specimen

Mode II loading may be induced when a cracked adhesive joint is subjected to bending. The mode II tests were conducted using ENF arrangement. Friction was not considered in this test. The tests were based on Ref. [9]. The specimens were loaded under displacement control at the rate of 1 *mm/min*. The critical load at delamination crack onset was recorded and loading was stopped as soon as evidence of crack propagation was confirmed by a load drop. Mode II strain energy release rate was calculated using [9]:

$$G_{IIC} = \frac{9a^2 P\delta}{2w\left(1/4L^3 + 3a^3\right)} x1000 \qquad (2)$$

where: G_{IIC} = Fracture toughness energy
δ = Cross head displacement at crack delamination onset
P = Critical load to start the crack
a = Initial crack length
w = Width of the specimen
L = Span length
The flexural modulus can be calculated from:

$$E_f = \frac{L^3}{4wt^3 C_0} \qquad (3)$$

where C_0 = Compliance obtain experimentally from the three-point bending test in the elastic range on the un-cracked specimen.

In the single lap tests, the initial grip separation was 75 *mm* with 25.4 *mm* in each sample end held in the machine grips. The load was applied at 13 *mm/min* according to the ASTM [10]. Three lap joints with variable overlap lengths were tested and load-displacement curves were recorded until the fracture was completely developed. Due to the geometrical eccentricity, the loaded specimens rotate as a result of the bending moment in order to align themselves in the load direction. The adherend rotation introduces peel stresses in the adhesive, which are most significant in the vicinity of the joint edges and eventually lead to failure of the adhesive joint. The results achieved from the experiments are discussed later in the paper.

3 Finite Element Modelling

The explicit finite element code, LS-Dyna, was used to perform the analysis. A Cohesive model was adopted for the analysis to represent failure along the bond line. The FE model was

designed to match the same slope and maximum load as those of the experiments. This was achieved by modelling the adhesive layer, tying the substrate materials, using a contact along the interface. Such a tied contact can be implemented as penalty formulation, where the adhesive nodal forces are functions of the relative displacement between the nodes. Friction was not considered in initial simulation. The penalty formulation used was linear elastic force displacement relation between the nodes, which can be represented by three orthogonal springs. The tied relation is defined as:

$$P_I = K_{IJ} D_J \qquad (4)$$

where: P_I = Force in direction I

D_J = Corresponding relative displacement between the two coincident nodes.

K_{IJ} = Diagonal matrix which complies with interpretation of the penalty formulation as three orthogonal springs.

The cohesive model used followed a linear traction-displacement law is defined by three parameters: the ultimate strength σ_0, the displacement which brings the stress to zero and the fracture energy G_C (Fig. 5). Data from modes I and II test are used to set realistic data for these three parameters.

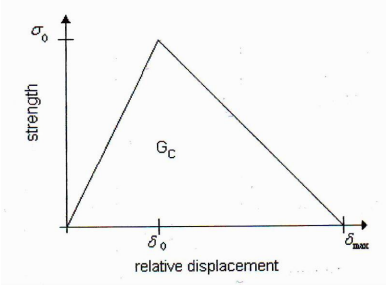

Fig. 5. Cohesive model

For all the FE models the mesh of the adherends consists of two dimensional four node isoparametric quadrilateral elements. The dimensions of the shells in the overlap area are constant while they increase along the laminate up to the free edges, as shown in Fig. 6, with an overlap length of 12.5 *mm*. The tabs were created of solid elements with a thickness of 2.86 *mm*. Due to the initially large simulation time, mass scaling was enforced to achieve a more reasonable computational time. To keep undesired effects of mass scaling in check, three simulations of each model were run. Figure 7 shows the load-displacement curves obtained for the model with 37.5 *mm* overlap. For the maximum load an error of 3% was recorded, which can be considered as acceptable. The mass scaling factor was 10^3.

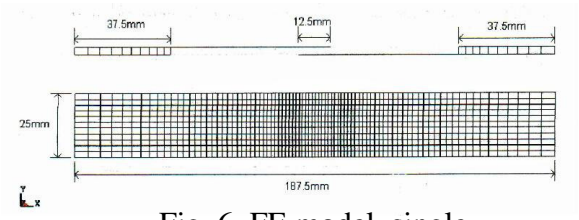

Fig. 6. FE model, single

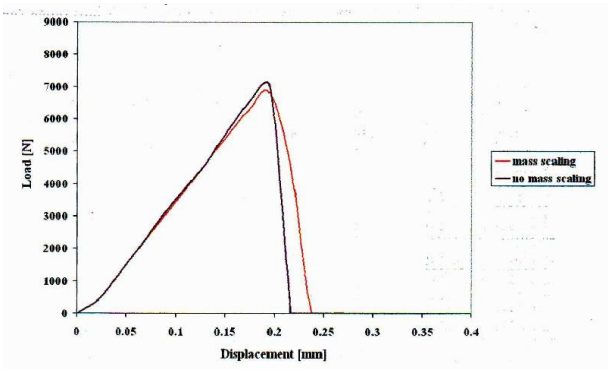

Fig. 7. Effect of mass scaling

Shell elements with a thickness of 2.86 *mm* were adopted to model the laminates. Tsai-Wu failure criterion was used for composite damage. The boundary conditions included rollers spread on the right tab with displacement applied horizontally, only on the 24 roller at the end of the tab, while the left tab was fixed. The displacement was applied at a constant rate of 13 *mm/s*. All master segment and slave segment contact types required were specified. Only slave nodes were checked for penetration through the master surface.

4 Experimental Results

The results of the mode I tests for all the specimens are shown in Table 9. It can be seen that there is a slight difference in the value of G_{IC} for 0/0 and 0/45 interfaces. Figure 8 plots the average value and standard deviation of G_{IC} for all the models tested. Figure 9 shows the load versus displacement curve recoded for mode II specimens. All the curves have same profile: the load increases linearly and then

displays non-linear behaviour that was physically evident through small crack propagation leading to load drops.

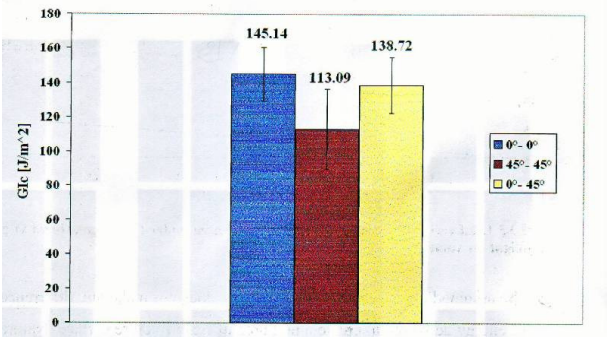

Fig. 8. G_{IC} test results

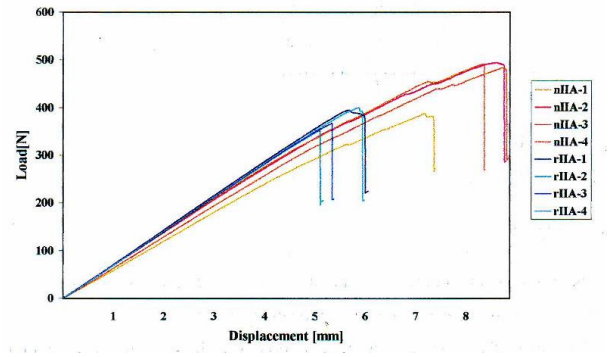

Fig. 9. Load vs displacement for mode II

Table 9 Energy release rate of mode I specimen

	Specimen	a [mm]	A [J]	G_{IC} [J/m^2]
0°-0°	IA1	101	0.41	163.9
	IA2	107	0.34	126.2
	IA3	116	0.41	141.7
	IA4	97	0.36	148.4
Mean				145.1
Standard deviation (SD)				15.6
45°-45°	IB1	101	0.26	103.1
	IB2	103	0.27	103.7
	IB3	99	0.24	97.1
	IB4	107	0.4	148.3
Mean				113.05
SD				23.69
0°-45°	IC1	97	0.36	147.7
	IC2	92	0.27	115.1
	IC3	97	0.37	152
	IC4	89	0.31	139.6
Mean				138.6
SD				16.49

The value of G_{IIC}, final crack length 'a_f' and the flexural modulus for release film and natural crack are presented in Tables 10 and 11, respectively.

Table 10 Values for release film specimen

Specimen	G_{IIC}[J/m^2]	a_f [mm]	E_f [GPa]
rIIA-1	1255	58.20	217
rIIA-2	1005	54.35	211
rIIA-3	1093	56.25	211
rIIA-4	1309	59.50	213
Average	1165.5	57.1	213.1
SD	141.2	2.3	3.1
rIIB-1	1068	61.35	168
rIIB-2	1315	61.80	161
rIIB-3	1202	63.50	170
rIIB-4	1374	63.75	168
Average	1239.7	62.6	166.7
SD	134.8	1.2	4.1
rIIC-1	1233	77.85	185
rIIC-2	1362	69.85	188
rIIC-3	1400	56.50	188
rIIC-4	1373	65.50	186
Average	1341.8	67.4	187
SD	74.4	8.9	1.6

Table 11 Values for natural crack specimen

Specimen	G_{IIC}[$J/m2$]	a_f [mm]	E_f [GPa]
nIIA-1	1558	58.30	182
nIIA-2	2367	61.00	206
nIIA-3	2350	59.20	196
nIIA-4	2285	59.50	212
Average	2140.2	59.5	198.9
SD	389.5	1.1	13.5
nIIB-1	561	54.30	137
nIIB-2	538	53.80	156
nIIB-3	837	54.00	125
nIIB-4	629	56.20	154
Average	641.1	54.6	143.1
SD	135.9	1.1	14.6
nIIC-1	2269	57.20	173
nIIC-2	2063	59.30	168
nIIC-3	1277	61.00	175
nIIC-4	2209	61.50	178
Average	1954.5	59.8	173.5
SD	460	1.9	4.3

The load versus displacement curves for single lap joints (A and C series) are shown in Fig. 10. Table 12 shows maximum load for single lap specimens.

Table 12 Single lap; Maximum load

Code	Maximum Load [*N*]
A1	5930
A2	5941
A3	5305
Average	5752
SD	364
B1	5955
B2	6195
B3	7209
Average	6453
SD	666
C1	8385
C2	7287
C3	6481
Average	7384
SD	956

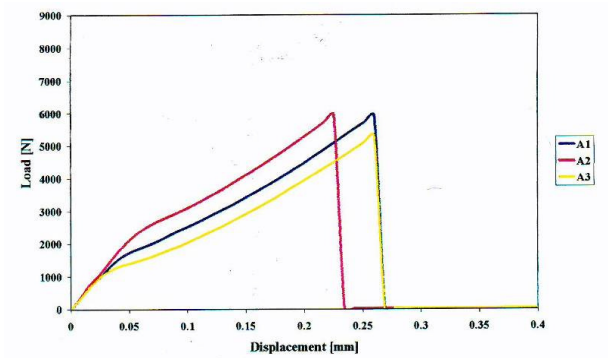

(a) A series specimens

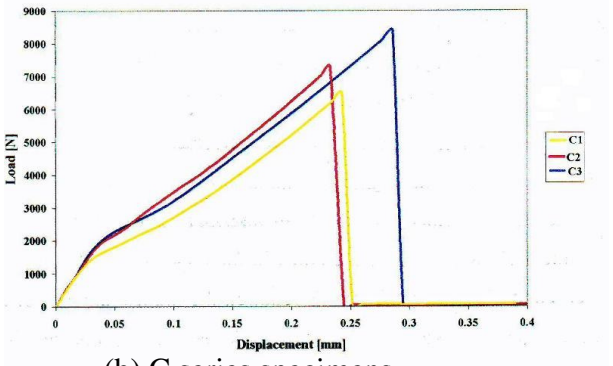

(b) C series specimens

Fig. 10. Load vs displacement for single lap

5 FEM results

The overall deformed shape of the single lap joint due to tensile load is shown in Fig. 11 for model A (12.5 *mm*) and C (37.5 *mm*). Similar results were achieved for model B (25 *mm*) but they are not depicted here. To better display the deformation of the laminates, displacements have been increased by a factor of 10. Table 13 shows the maximum load, stiffness and energy for FE analysis.

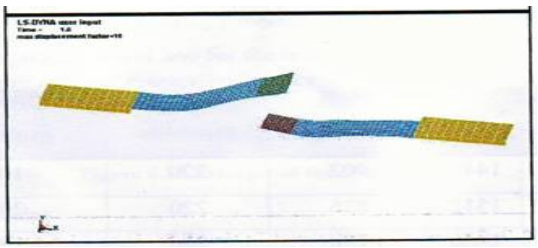

(a) Model A, final failure

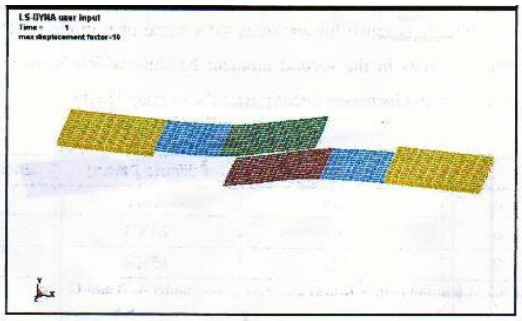

(b) Model C, final failure

Fig. 11. Final failure using FE modelling

Table 13 FE results for models A, B and C.

	Max Load [*N*]	Stiffness [*N/mm*]	Energy [*Nmm*]
A	5435	18878	1007
B	5567	26954	659
C	6803	35104	826

6 Discussion

The specimen with $0^o/0^o$ interface reaches the highest value of G_{IC} (Fig. 8). However, the difference between the energy values for $0^o/0^o$ and $0^o/45^o$ is quite low to allow any significant conclusion. It can be assumed that having $0^o/0^o$ and $0^o/45^o$ makes a small difference in terms of energy delivered to create a unit area of fresh fracture surface. Low G_{IC} value for $45^o/45^o$ can be due to possible errors during lay up process. Additional trials are required to help draw a clearer conclusion. After the failure, specimens were peeled and bonded areas were inspected. As depicted in Fig. 12, for A1 and most of the other specimens crack tends to jump from one interface to the other, producing an “alternating crack path”. The crack started from the weakest point at the tip of the specimen and propagated along the layer between the adhesive and

adherends, which represents the lowest fracture toughness layer. It can be stated that adhesive did not seem to have created a strong chemical link with the substrate during the curing process. This was confirmed by the clean failure of specimen C3, as shown in Fig. 12, which can be attributed to weak interfacial bonding forged during the recommended cure process.

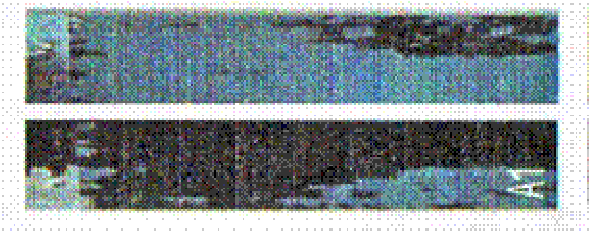

(a) Alternating crack path

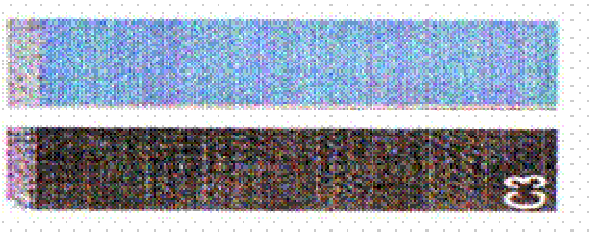

(b) Adhesive failure

Fig. 12. Different failure modes.

From Tables 10 and 11, the following observations can be made:

- The value of crack initiation from the Release Film specimens were lower than the equivalent values from the Natural Crack ones, suggesting that the insert film used during the lay-up generated sharp initial crack which yielded lower initiation G_{IIC} than the others.
- The values found for all the Release Film specimens were more conservative.

The Natural Crack specimens with the 45o/45o orientation showed about 70% reduction in value of GIIC compared to 0o/0o and 0o/45o specimen. During C-scan and forced peeling after experiments it was found that the length of the natural crack for 45o/45o specimen is about half the length when compared with other specimens. The occurrence of shorter crack length and low value of GIIC was deemed to be due to a weak bond which did not require a high energy level to instigate the crack.

For single lap joints, as shown in Fig. 10, the first change in the slope was due to slippage at the grips, after which the structure carried the increasing load until failure. It can be seen that the maximum failure load increases with an increase in overlap length. Most failed surfaces display adhesive failure only. No cohesive failure was observed in these specimens. Only specimens A3 and C3 show "crack leaps" across the adhesive (see Fig. 13).

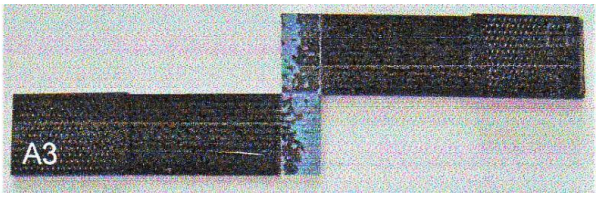

(a) Model A3

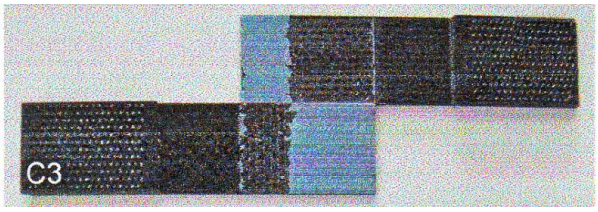

(b) Model C3

Fig. 13. Shear lap failure

The initial FE analysis captured the contact failure sequencing in single lap joints. The failure started from the corners of the bonded area (the high stress region) moving towards the centerline of the model. This phenomenon was also recorded during experimental analysis. The load versus displacement graph for the model is shown in Fig. 14. It can be seen that, similar to the experimental results, the load increases with the overlap length. It can further be noted that failure displacement reduces as the overlap length increases. The FE results compare well with the experimental data as shown in Fig. 15. The values of maximum load and stiffness from FE and experimental analysis are provided in Tables 14 and 15. The maximum error recorded for maximum load was 14%, which could be improved by increasing the batch size. In the case of maximum load, the FE models provided conservative solution. Stiffness comparison showed good correlation between the results of specimens A and B. The larger stiffness variations, compared to those of specimens A and B, require further investigation.

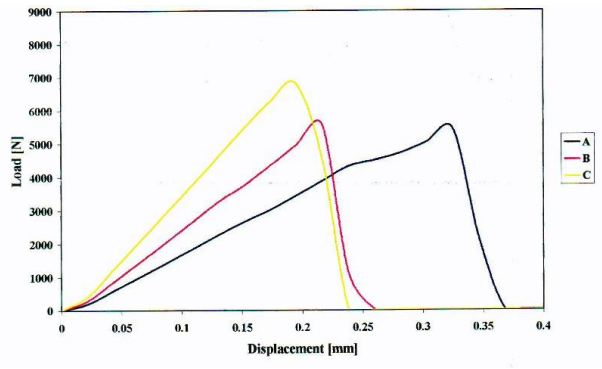

Fig. 14. Effect of overlap length on failure load

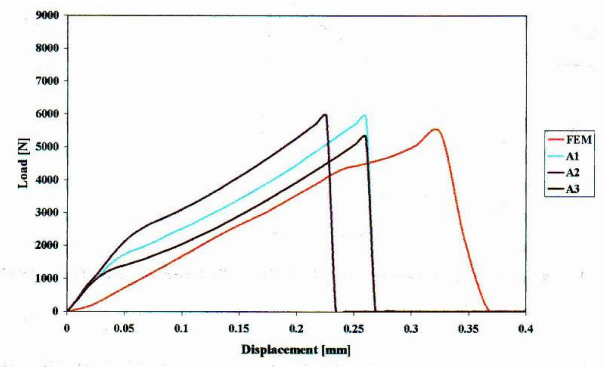

(a) FEM vs. experiments for model A

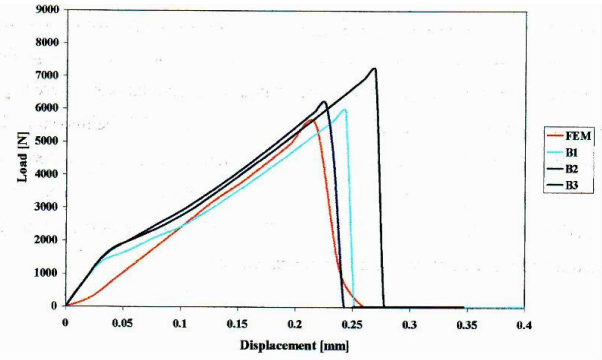

(b) FEM vs. experiments for model B

Fig. 15. FEM vs. experiments

Table 14 Maximum load comparison

Model	EXP max. load [*N*]	FEM max. load [*N*]	Error %
A	5725	5435	-5
B	6453	5567	-14
C	7384	6803	-8

Table 14 Stiffness comparison

Model	EXP Slope Avg. [*N/mm*]	FEM slope [*N/mm*]	Error %
A	20524	18878	-8
B	26307	26954	2.4
C	27648	35104	21

7 Conclusion

Experimental tests and FE analysis were conducted on composite bonded joints. The effect of different ply orientations ($0^o/0^o$, $0^o/45^o$ and $45^o/45^o$) on delamination at the interface of the adherend and adhesive was investigated. For mode I tests, it was found that different interfacial orientations did not significantly influence the energy required to create a unit area of fresh fractured surface. Mode II tests were conducted on Release Film and Natural Crack specimens. The results of the analysis show that the specimens with release film produce more conservative and lower values of G_{IIC} when compared to natural crack specimens.

Two-dimensional shell models of the single lap joints were created in an explicit FE code, LS-Dyna. The values of G_{IC} and G_{IIC} were used to model the adhesive as a contact between the laminates. Simulation results were compared with experimental tests conducted on single lap joints with variable overlap lengths (12.5 *mm*, 25 *mm* and 37.5 *mm*). The load-displacement data obtained from the experiments were in close agreement with the numerical results. The rather high average error recorded in the experimental trial for maximum stiffness and maximum load was attributed to the small specimen batch sizes and their resulting large standard deviation.

Following recommendations can be made for future work:

- Use of different adhesive for similar joint configurations may provide further insight into failure mechanism of the joints.
- Construction of three-dimensional simulation models, in which adhesive is modelled as a specific material with an appropriate damage formulation, can also offer a more comprehensive understanding of the failure mechanism. This practice is currently underway.

References

[1] Pandey, PC, Shankaragouda, H & Singh, AK. 'Nonlinear analysis of adhesively bonded lap joints considering viscoplasticity in adhesives', Computers and Structures, vol. 70, pp. 387-413, 1999.

[2] Savage, G, 'Failure prevention in bonded joints on primary load bearing structures', Engineering failure Analysis, vol. 14, pp. 321-48, 2007.

[3] Her, S-C, 'Stress analysis of adhesively-bonded lap joints', Composite Structures, vol. 47, pp. 673-8, 1999.

[4] Hiley, MJ, 'Delamination between multi-directional ply interfaces in carbon-epoxy composites under static and fatigue loading', Fracture of polymers, vol. 27, pp. 61-72, 2000.

[5] Yan, C, Mai, WY & Ye, L, 'Effects of constraint on crack tip stress fields and fracture toughness in adhesive joints.' *Fracture of polymers, Composites and Adhesives*, vol. 27, pp. 307-16, 2000.

[6] Hart-Smith, L, *Adhesive-bonded single-lap joints*, CR-112235 NASA Langley Research Center, 1973.

[7] Volkersen, O, 'Die nietkraftverteilung in zugbeanspructen nietverbindungen mit konstanten laschenquerschnitten.' *Luftfarhrtforschung*, vol. 15, pp. 41-7, 1938.

[8] DIN EN 6033. ICS 49.040.10. Aerospace series-Carbon fiber reinforced plastic-Test method-Determination of interlaminar fracture toughness energy-Mode I – G_{IC}. May 1996.

[9] DIN EN 6034. ICS 49.040.10. Aerospace series-Carbon fiber reinforced plastic-Test method-Determination of interlaminar fracture toughness energy-Mode II – G_{IIC}. May 1996.

[10] ASTM Designation: D 5868 – 01 '*Standard method for lap shear adhesion for fiber reinforced plastic (FRP) bonding*'.

Acknowledgements

The authors would like to acknowledge the great technical support provided by Messrs T. Rosewarne and P. Tkatchyk from the School of Aerospace, Mechanical and Manufacturing Engineering of the Royal Melbourne Institute of Technology in relation to conducting experimental work. The constructive comments received from Dr A. Gunnion and Mr D. Elder from the Cooperative Research Centre for Advanced Composite Structures have also been instrumental and are appreciated.

Copyright Statement